DOI:
10.1161/CIRCIMAGING.114.002417

Document Version
Publisher's PDF, also known as Version of record

OPEN

Monitoring Vascular Permeability and Remodeling After Endothelial Injury in a Murine Model Using a Magnetic Resonance Albumin-Binding Contrast Agent

Begoña Lavin, PhD*; Alkystis Phinikaridou, PhD*; Silvia Lorrio, PhD; Carlos Zaragoza, PhD¶; René M. Botnar, PhD¶

Background—Despite the beneficial effects of vascular interventions, these procedures may damage the endothelium leading to increased vascular permeability and remodeling. Re-endothelialization of the vessel wall, with functionally and structurally intact cells, is controlled by endothelial nitric oxide synthase (NOS3) and is crucial for attenuating adverse effects after injury. We investigated the applicability of the albumin-binding MR contrast agent, gadofosveset, to noninvasively monitor focal changes in vascular permeability and remodeling, after injury, in NOS3-knockout ($NOS3^{-/-}$) and wild-type (WT) mice in vivo.

Methods and Results—WT and $NOS3^{-/-}$ mice were imaged at 7, 15, and 30 days after aortic denudation or sham-surgery. T_1 mapping ($R_1=1/T_1$, s^{-1}) and delayed-enhanced MRI were used as measurements of vascular permeability (R_1) and remodeling (vessel wall enhancement, mm^2) after gadofosveset injection, respectively. Denudation resulted in higher vascular permeability and vessel wall enhancement 7 days after injury in both strains compared with sham-operated animals. However, impaired re-endothelialization and increased neovascularization in $NOS3^{-/-}$ mice resulted in significantly higher R_1 at 15 and 30 days post injury compared with WT mice that showed re-endothelialization and lack of neovascularization (R_1 [s^{-1}]=15 days: $_{NOS3}{}^{-/-}$4.02 [interquartile range, IQR, 3.77–4.41] versus $_{WT}$2.39 [IQR, 2.35–2.92]; 30 days: $_{NOS3}{}^{-/-}$4.23 [IQR, 3.94–4.68] versus $_{WT}$2.64 [IQR, 2.33–2.80]). Similarly, vessel wall enhancement was higher in $NOS3^{-/-}$ but recovered in WT mice (area [mm^2]=15 days: $_{NOS3}{}^{-/-}$5.20 [IQR, 4.68–6.80] versus $_{WT}$2.13 [IQR, 0.97–3.31]; 30 days: $_{NOS3}{}^{-/-}$7.35 [IQR, 5.66–8.61] versus $_{WT}$1.60 [IQR, 1.40–3.18]). Ex vivo histological studies corroborated the MRI findings.

Conclusions—We demonstrate that increased vascular permeability and remodeling, after injury, can be assessed noninvasively using an albumin-binding MR contrast agent and may be used as surrogate markers for evaluating the healing response of the vessel wall after injury. **(*Circ Cardiovasc Imaging*. 2015;8:e002417. DOI: 10.1161/CIRCIMAGING.114.002417.)**

Key Words: gadofosveset trisodium ■ magnetic resonance imaging ■ permeability ■ vascular remodeling

Despite the beneficial effects of percutaneous transluminal coronary angioplasty and stent implantation, these procedures may damage the vessel wall, particularly the endothelial layer, leading to increased vascular permeability and remodeling. Therefore, noninvasive assessment of these processes may provide a more comprehensive understanding of the focal responses of the vessel wall to injury.

See Clinical Perspective

In healthy vessels, functional endothelium produces nitric oxide through endothelial nitric oxide synthase (eNOS or NOS3). Nitric oxide controls the vasoreactivity of the vessel wall, inhibits platelet and leukocyte adhesion and smooth muscle cell proliferation and migration, promotes re-endothelialization, and regulates endothelial cell and tight junction morphology and vascular permeability.[1,2] Dysfunctional endothelium because of vascular injury or cardiovascular risk factors[3–7] is characterized by reduced NOS3-derived nitric oxide resulting in the attenuation of endothelial-dependent vasodilation[5,8] and accelerated vascular remodeling.[9–12]

Genetically modified $NOS3^{-/-}$ mice (1) vasodilate only in response to endothelial-independent stressors,[13] (2) have

Received July 23, 2014; accepted March 20, 2015.

From the Division of Imaging Sciences and Biomedical Engineering, King's College London, King's Health Partners, St. Thomas' Hospital, London, United Kingdom (B.L., A.P., S.L., R.M.B.); The British Heart Foundation Centre of Excellence, Cardiovascular Division (B.L., A.P., R.M.B.) and Wellcome Trust and EPSRC Medical Engineering Center (B.L., R.M.B.), King's College London, London, United Kingdom; Cardiovascular Research Unit, University Francisco de Vitoria/Hospital Ramón y Cajal, Ctra. Colmenar Viejo, km 9,100, Madrid 28034, Spain (C.Z.).

*Drs Lavin and Phinikaridou have contributed equally to the preparation of this article.

¶Drs Zaragoza and Botnar contributed equally to this work.

The Data Supplement is available at http://circimaging.ahajournals.org/lookup/suppl/doi:10.1161/CIRCIMAGING.114.002417/-/DC1.

Correspondence to Begoña Lavin, PhD, Division of Imaging Sciences and Biomedical Engineering, King's College London, St. Thomas' Hospital, 4th Floor, Lambeth Wing, London SE1 7EH, United Kingdom. E-mail bego.1.lavin@kcl.ac.uk

impaired re-endothelialization,[12,14,15] and (3) have increased inflammatory response after injury[12,16] collectively leading to increased vascular remodeling.[10–12] However, despite some of the similarities between the vascular response observed in NOS3$^{-/-}$ and patients that undergo percutaneous interventions, endothelial denudation followed by vascular remodeling, as seen in this model, may represent the worst case outcome compared with human interventions. Interestingly, in a rabbit model, viral and nonviral transfection of NOS3 and placement of NOS3 gene–eluting stents significantly reduced vascular remodeling and improved re-endothelialization.[14,15,17]

Uptake into the vessel wall of albumin-binding dyes (Evans blue, ^{128}I-albumin, rhodamine) has been traditionally used as a surrogate marker of vascular permeability in ex vivo experiments.[18] MRI is a noninvasive modality that allows the study of both endothelial function[19–21] and vascular remodeling with high spatial resolution.[22–25] An albumin-binding MRI contrast agent, gadofosveset, has been recently used as the in vivo counterpart of albumin-binding dyes and allowed the assessment of focal changes in vascular permeability and vascular remodeling in atherosclerosis,[25–28] stent-induced vascular remodeling,[27] and chronic myocardial infarction.[29] Gadofosveset is a clinically approved gadolinium-based, blood pool contrast agent. After injection in mice, ≈70% of circulating gadofosveset binds reversibly to serum albumin and this increases its r_1 relaxivity by 5- to 10-fold (r_1=25 mmol L^{-1} s^{-1}) compared with the free fraction (r_1=5 mmol L^{-1} s^{-1}).[30,31] Uptake of gadofosveset into the vessel wall of pathological tissues has been shown to occur through damaged endothelium[32,33] and leaky neovessels.[26,27]

Endothelial damage and vascular remodeling may occur after vascular injury. Re-endothelialization of the vessel wall with functionally and structurally intact endothelial cells is crucial for minimizing vascular remodeling and maintaining the long-term patency of the treated vessel. We hypothesized that augmented vascular permeability because of impaired re-endothelialization and increased neovascularization, observed after injury in the NOS3$^{-/-}$ mice,[12] is associated with enlarged vascular remodeling that could be monitored noninvasively using gadofosveset-enhanced MRI in vivo.

Methods

Animals/Endothelial Denudation

Wild-type (WT) C57BL/6 mice and B6.129P2-Nos3^{tm1Unc}/J knock-out mice (8–12 weeks old) were purchased from the Jackson Laboratory (Bar Harbor, ME). Surgery was performed under isoflurane anesthesia using a dissection microscope (Leica, Wetzar, Germany). Before surgery, the abdominal fur was removed with lotion hair and the surgical field was disinfected. After a midline incision of the abdomen, the aorta, renal, and iliac arteries were exposed and isolated. Subsequently, 2 ligatures (surgical silk, size 4-0, Aragó, Zaragoza, Spain) were placed around the aorta, below the renal arteries, and above the iliac bifurcation, respectively (Figure 1A; left). A 30G syringe was introduced into the abdominal aorta via an aortic puncture followed by a bolus infusion of 1-mL saline buffer. This procedure was repeated 3× to remove the endothelial cells (Figure 1A; right). Finally, the needle was removed, the aortic puncture was repaired, and the ligatures were removed to restore blood flow. The muscle and skin incisions were sutured (5-0 Vicryl, Ethicon Inc, Somerville, NJ), and the animals were allowed to recover. Each surgery lasted 30 minutes. Sham-operated animals underwent the same surgical procedure described above without injuring the endothelial layer. All procedures used in these studies were performed in accordance with the guidelines of the UK Home Office.

In Vivo MRI Protocol at 3T

In vivo vessel wall imaging was performed using a Philips Achieva MR scanner (Philips Healthcare, Best, The Netherlands) equipped

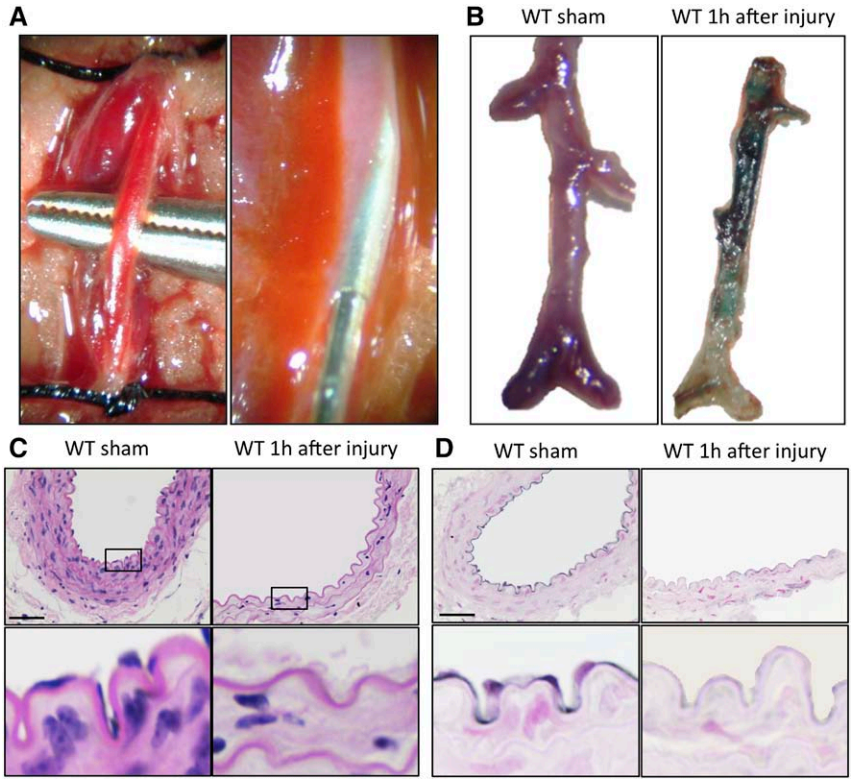

Figure 1. Endothelial denudation model. **A** (**left**), Isolation and temporal obstruction of blood flow in the abdominal aorta between renal arteries and iliac bifurcation. **A** (**right**), Infusion of saline solution (0.9% NaCl) with a 30G syringe to denudate vascular endothelial cells. **B**, In situ Evans blue dye staining shows increased vessel permeability in animals 1 hour after injury when compared with sham-operated mice (n=4). **C**, Hematoxylin and eosin staining showing the presence of endothelial cells in sham-operated animals (**left**) and the absence of endothelial cells 1 hour after injury (**right**) in wild-type (WT) animals (n=3). **D**, Corresponding immunohistochemistry for PECAM-1 shows a significant decrease of endothelial cells in injured compared with sham-operated animals (n=3). **E**, Scale bars correspond to 0.3 mm.

with a clinical gradient system (30 mT m^{-1}, 200 mT m^{-1} ms^{-1}) and a single-loop surface coil (diameter=47 mm). Mice were imaged before, 7, 15, and 30 days after the surgery (Figure I in the Data Supplement). Four sham-operated mice and 6 injured mice per strain were imaged per time point. Animals were imaged in supine position before and 30 minutes after intravenous administration of 0.03 mmol/kg gadofosveset (Lantheus Medical Imaging, North Billerica, MA). Anesthesia was induced with 5% and maintained with 1% to 2% isoflurane during the MRI experiments. After 3-dimensional (3D) gradient echo scout scans, contrast-enhanced angiography images were acquired for visualization of the vasculature with a field of view (FOV)=35×35×16 mm, matrix=232×233, in-plane resolution=0.15×0.15 mm, slice thickness=0.5 mm, repetition time/echo time (TR/TE)=28/6 ms, and flip angle=40°. The maximum intensity projection images were used to plan the subsequent delayed enhancement (DE) and T_1 mapping scans. A 2D-Look–Locker sequence planned perpendicular to the aorta was used to determine the optimal inversion time (TI) for blood signal nulling. Acquisition parameters were FOV=30×30 mm, matrix=76×75, in-plane resolution=0.4×0.4 mm, slice thickness=2 mm, TR/TE=18/8.3 ms, TR between subsequent IR pulses=1000 ms, and flip angle=10°. An inversion-recovery 3D fast gradient echo sequence was acquired 30 minutes post injection and was used for DE-MRI and visualization of contrast uptake. Imaging parameters were FOV=35×35×12 mm, matrix=348×348, in-plane resolution=0.1×0.1×1 mm (normal vessel wall thickness=0.2 mm), slices=24, TR/TE=27/8.2 ms, TR between subsequent infrared pulses=1000 ms, and flip angle=30°. T_1 mapping was performed using a sequence that uses 2 nonselective inversion pulses each followed by 8-segmented readouts. The 2 imaging trains result in a set of 16 images per slice with increasing inversion times ranging from 20 to 2000 ms. For T_1 mapping, the acquisition parameters were FOV=36×22×10 mm, matrix=180×102, in-plane resolution=0.2×0.21×0.5 mm, slices=20, TR/TE=9/4.6 ms, and flip angle=10°. R_1 values were computed on a pixel-by-pixel basis using in house Matlab software.[24]

MRI Data Analysis

Vascular remodeling was calculated by manually segmenting the visually contrast-enhanced area of the vessel wall as seen on the DE-MRI images using OsiriX (OsiriX Foundation, Geneva, Switzerland). To ensure that the segmented area encompassed the vessel wall, the DE-MRI images were coregistered and fused with the magnetic resonance angiographic images. DE-MRI areas were measured on consecutive slices along the aorta and were added for each animal to express the total extent of vessel wall remodeling. R_1 values were measured on consecutive slices along the aorta and were averaged for each animal.

Histology

Tissue Harvesting

For all histological procedures, mice were anesthetized with isoflurane and perfused through the left ventricle with physiological saline (for transmission electron microscopic [TEM] studies and Evans blue dye [EBD] staining) or with physiological saline followed by 10% buffered formalin (for hematoxylin and eosin [H&E] staining and immunohistochemistry).

EBD Staining

Vascular permeability was assessed by visualizing and quantifying the leakage of EBD into the vessel wall. Mice were anesthetized, and EBD (0.1 mL of 1% dye in saline) was injected in the left ventricle. After 10 minutes, the injured abdominal aorta was isolated, dried, and weighed. EBD was extracted by incubation in formamide for 24 hours at 60°C and the absorbance was measured at 620 nm. Standard curves for pure EBD were used to calculate the total amount of dye in the tissue. Four animals were analyzed per group at each time point.

H&E staining and immunohistochemistry

Abdominal aortas were fixed in 10% buffered formalin for 48 hours at 4ºC, embedded in paraffin, and sectioned transversely (5-μm thick). H&E staining was used to investigate vessel wall morphology. Immunohistochemistry using antibodies to platelet endothelial cell adhesion (PECAM-1; 1:50, BD Pharmingen, Oxford, UK) and serum albumin (1:5000, Abcam, Cambridge, UK) was used to study endothelial cells and serum albumin present in the vessel wall, respectively. Five slices (5 μm) were stained per animal. Digital images were used to analyze the histological sections using ImageJ (NIH).

Vascular remodeling was used to describe 2 changes that occur in the vessel wall after injury: neointima formation that involves the inward deposition of cellular components and extracellular matrix proteins at the luminal surface, and the accumulation of extracellular matrix/collagen and neovessels at the periphery of the adventitial contour of the vessel wall. Vascular remodeling was calculated using the H&E images [adventitia area−the luminal area (mm^2)]. Immunopositive areas were analyzed on digital images by computerized planimetry. The immunopositive area was segmented on the images and expressed as normalized albumin area (%; albumin immunopositive area/area of vascular remodeling)×100. Individual measurements performed within each animal were averaged and 4 animals were analyzed per group at each time point.

Transmission Electron Microscopy

Preselected segments of the aorta that showed enhancement on MRI (n=1 per time point per group) were pinned down and fixed in 2% glutaraldehyde in 0.1 mol/L sodium phosphate buffer (pH 7.4) for 2 hours, washed with sodium phosphate buffer for 2 hours, and post fixed in 1% OsO_4 for 2 hours. Each aorta was divided into 3 levels (upper, middle, and low) starting from the left renal branch to the iliac bifurcation and processed for histological analysis. Subsequently, 3 sections were examined from the aorta of each animal. Samples were dehydrated through a graded series of ethanol and embedded in epoxy resin. Semithin sections (0.2 μm) were stained with toluidine blue for light microscopy examinations and were used to guide sampling for TEM studies. Thin sections (0.09 μm) were collected on 150 mesh copper grids and double stained with uranyl acetate and lead citrate for electron microscopy examinations (H7650, Hitachi, Tokyo, Japan).

Statistical Analysis

GraphPad Prism 5.00 was used for the statistical analysis. Two-group comparisons of continuous variables were performed with a Mann–Whitney nonparametric exact test after the variables were ranked. The data are presented as the median±interquartile range, and P values <0.05 were used to define statistical significance.

Results

Endothelial Denudation Protocol

Histological validation and characterization of the surgical protocol was shown in our previous work, where we show that this procedure removes virtually all endothelial cells over the

area being subjected to the saline infusion procedure.[12] Representative images of the surgical protocol are illustrated in Figure 1A. EBD staining, a histological marker of endothelial permeability, was performed in a subgroup of WT animals, showing endothelial denudation 1 hour after surgery. En face photographs of the extracted aortas showed increased uptake of EBD demonstrating higher vascular permeability in injured animals compared with the sham-operated mice (Figure 1B). H&E staining and PECAM-1 immunohistochemistry further demonstrate that the endothelium was successfully removed after vascular injury compared with sham-operated animals (Figure 1C and 1D).

MRI Findings

Vascular permeability was measured using relaxation rate (R_1) maps that allow in situ quantification of the gadolinium concentration in the vessel wall (Figure 2). This analysis revealed significantly higher R_1 in denudated animals, in both strains, 7 days after injury compared with sham-operated mice. Importantly, NOS3$^{-/-}$ mice showed significantly higher R_1 15 and 30 days after injury compared with WT mice that show restoration of the R_1 values close to baseline (Figure 2; graph). These results suggest healing of the vessel wall and normalization of vascular permeability in WT whereas in NOS3$^{-/-}$ mice vascular permeability remained increased after injury.

Vascular remodeling was quantified using DE-MR images after administration of gadofosveset. Similar to the R_1 values, DE-MRI areas were higher in the abdominal aorta of both WT and NOS3$^{-/-}$ mice 7 days after injury compared with sham-operated animals (Figure 3, second row). Importantly, in NOS3$^{-/-}$ mice, the area of vessel wall enhancement remained higher 15 and 30 days after injury compared with

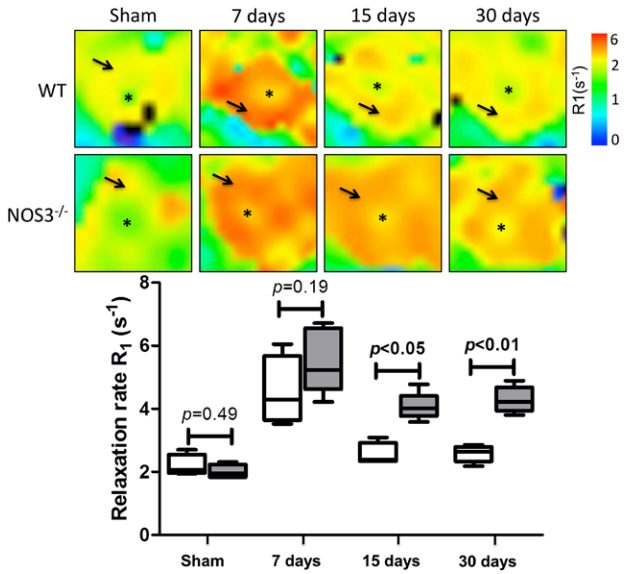

Figure 2. Vascular permeability is higher in NOS3-knockout (NOS3$^{-/-}$) mice after aortic endothelial denudation, as measured by gadofosveset uptake. Cross-sectional relaxation rate (R_1) mapping of the abdominal aorta at different time points. First row, wild-type (WT) animals and second row, NOS3$^{-/-}$ mice. Asterisks indicate aortic lumens; arrows indicate aortic vessel walls. The bar graph shows quantification of vessel wall R_1 as measured by MRI (n=6). NOS3 indicates endothelial nitric oxide synthase.

that observed in WT mice at the same time points (Figure 3, third and fourth rows). The area of vessel wall enhancement in WT mice 15 and 30 days post injury was similar to that observed in sham-operated animals (Figure 3, first column). The quantitative changes in the DE-MRI area are also illustrated (Figure 3; graph). Finally, correlation analysis showed a strong linear correlation between DE-MRI and R_1 (r=0.702; P<0.001; Figure IIA in the Data Supplement). Collectively, these data suggest that the differential response in vascular permeability and remodeling, after injury, between NOS3$^{-/-}$ and WT can be assessed noninvasively by R_1 mapping and DE-MRI after gadofosveset administration.

Histological Findings

Ex vivo histological analysis corroborated the in vivo MRI data. EBD (Figure 4A) and albumin immunohistochemistry (Figure 4B) showed that at 7 days after injury both NOS3$^{-/-}$ and WT had focal uptake of the dye and albumin immunopositive areas indicating uptake of the EBD and albumin into the vessel wall because of increased vascular permeability. However, NOS3$^{-/-}$ showed persistent and significantly higher uptake of EBD and albumin in the injured segment of the abdominal aorta at 15 and 30 days post injury compared with WT mice. Vessels from sham-operated mice, of both strains, showed low uptake of EBD and albumin immunopositive areas located primarily in the adventitial layer and to a lesser extent in the endothelium.

PECAM-1 immunohistochemistry showed impaired re-endothelialization in NOS3$^{-/-}$ compared with WT mice after injury (Figure 5A). Furthermore, PECAM-1 immunohistochemistry revealed neovessel formation within the remodeled area (Figure 5B), breaks in-between adjacent endothelial cells (Figure 5C), and regions of denudation (Figure 5D) in NOS3$^{-/-}$ mice but not in WT mice, which showed complete re-endothelialization 30 days after surgery (Figure 5E). H&E staining showed increased vascular remodeling in NOS3$^{-/-}$ compared with WT mice after injury (Figure 5F). Quantitative differences in vessel wall area between the 2 mice strains were significant at 7, 15, and 30 days post injury (Figure 5F; graph).

Qualitative ultrastructural changes after vessel wall injury were studied with TEM (Figure III in the Data Supplement). At 7 days post injury, the endothelial layer was absent in both strains. In WT mice, the vessel wall was re-endothelialized with endothelial cells that appeared elongated and had cytoplasmic vacuolization and microvilli at 15 and 30 days. Conversely, NOS3$^{-/-}$ mice showed re-endothelialization with cuboidal endothelial cells and partial fragmentation of elastin fibers.

Correlation analysis between the MRI measurements and histology showed a strong linear correlation between the vessel wall R_1 and EBD uptake (r=0.782; P<0.001; Figure IIB in the data Supplement) and between the R_1 and normalized albumin area (r=0.83; P<0.001; Figure IIC in the Data Supplement). There was also a statistically significant correlation between EBD and normalized albumin area (r=0.80; P<0.001; data not shown). The correlation between the DE-MRI and histology was not statistically significant when all time points after injury were included (r=0.41; P=0.02; Figure IID in the Data Supplement). However, the correlation was significant

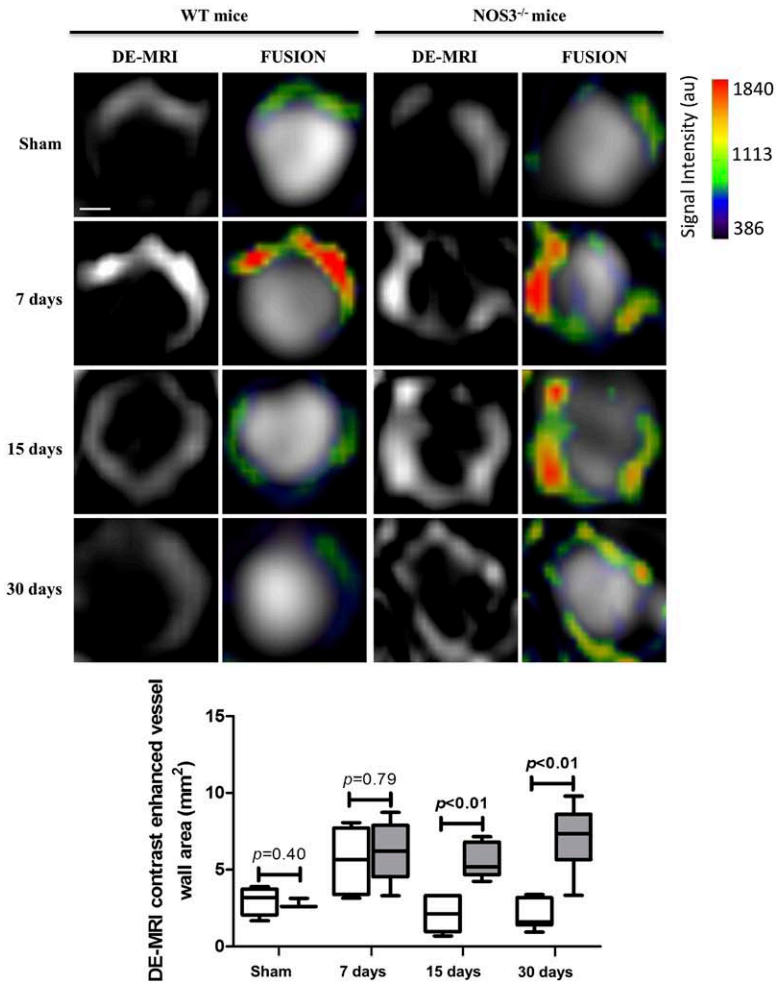

Figure 3. Vessel wall gadofosveset enhancement is higher in NOS3-knockout (NOS3$^{-/-}$) mice after aortic endothelial denudation. First and third columns, wild-type (WT) and NOS3$^{-/-}$ cross-sectional delayed-enhancement MR images (DE-MRI) of the abdominal aorta. Second and fourth columns, corresponding WT and NOS3$^{-/-}$ DE-MRI fused with magnetic resonance angiography images. NOS3$^{-/-}$ mice after vascular injury show persistent gadofosveset enhancement, whereas WT animals show decreased gadofosveset enhancement over time. Bar graph shows quantification of the contrast-enhanced vessel wall area as measured by MRI (n=6). Scale bar corresponds to 0.3 mm. NOS3 indicates endothelial nitric oxide synthase.

(r=0.78; P<0.001; Figure IID in the Data Supplement) after the acute phase (7 days), when measurements derived from sham-operated animals and at 15 and 30 days post injury were included.

Discussion

In this study, we investigated the applicability of the albumin-binding MR contrast agent, gadofosveset, to noninvasively monitor focal changes in vascular permeability and remodeling, after injury, in NOS3-knockout (NOS3$^{-/-}$) and WT mice in vivo. We demonstrate that (1) increased vascular permeability, measured in situ using T_1 mapping, showed higher vessel wall R_1 rates in NOS3$^{-/-}$ mice at 15 and 30 days postinjury compared with WT animals, and correlated with measures of vascular permeability, including EBD and albumin immunohistochemistry. In addition, histological staining, including PECAM-1, showed impaired re-endothelialization and neovessel formation in NOS3$^{-/-}$ compared with WT animals. (2) DE-MRI using an albumin-binding contrast agent, gadofosveset, enables in vivo quantification of vascular remodeling after injury. NOS3$^{-/-}$ mice showed significantly larger vascular remodeling, measured as increased contrast-enhanced area by MRI, compared with WT animals 15 and 30 days after injury. Ex vivo H&E validated the presence of extensive vascular remodeling in NOS3$^{-/-}$ mice compared with WT animals. We propose that uptake of gadofosveset into the vessel wall measured with T_1 mapping and DE-MRI could provide surrogate markers to assess the healing response of the vessel wall in response to vascular injury.

Several experimental murine models of induced vascular injury have been described.[34–37] Arterial ligation and mechanically induced denudation are among the 2 most common procedures. Although the model of arterial ligation provided important insights in the biological processes involved in vascular remodeling, it did not allow evaluation of the role of the endothelium that was 1 of the primary goals of our study. Mechanically induced vascular injury using guide wires causes endothelial denudation but it could also tear the elastic lamina. To overcome this complication, non–guide wire methods have been developed[12,36] that showed similar histological vessel wall changes to those observed after percutaneous interventions, both in animal models[37,38] and humans.[39] Particularly, using a non–guide wire surgical procedure, we characterized the differences in the vascular response between NOS3$^{-/-}$ and WT mice by histology.[12]

In our study, we found that the highest vascular permeability occurred 7 days after vascular injury, as measured by in vivo and ex vivo methods, and was similar between the 2 strains. However, in vivo measurements of vascular remodeling, as measured by DE-MRI at 7 days overestimated the vessel wall area compared with that measured by H&E staining.

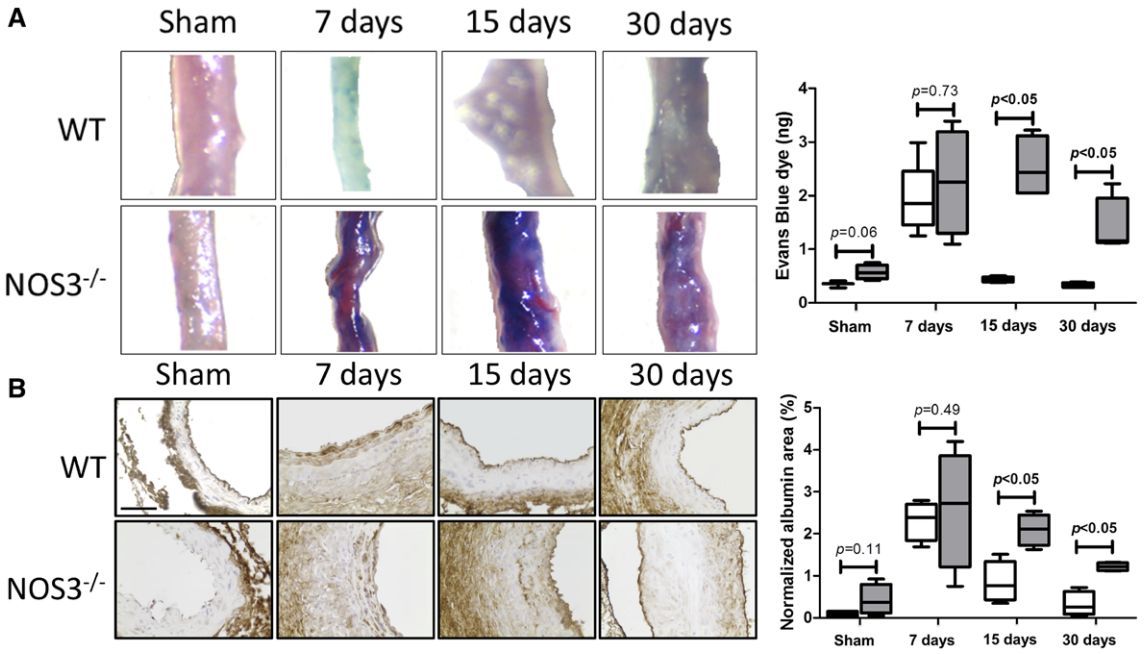

Figure 4. Vascular permeability is higher in NOS3-knockout (NOS3$^{-/-}$) mice after endothelial denudation. **A**, In situ Evans blue dye (EBD; n=4) shows a persistent leakage of EBD into the vessel wall in NOS3$^{-/-}$ mice after vascular injury, whereas wild-type (WT) mice show normalization over time. **B**, Serum albumin immunohistochemistry (n=4) in WT and NOS3$^{-/-}$ mice shows increased albumin leakage into the vessel wall in NOS3$^{-/-}$ when compared with WT mice after injury. Scale bar corresponds to 0.3 mm. NOS3 indicates endothelial nitric oxide synthase.

This might be because of the lack of the endothelial barrier, which allows for unobstructed leakage of molecules in the blood (eg, albumin, gadofosveset) into the vessel wall, leading to high permeability that is not necessarily accompanied by the presence of vascular remodeling. This data suggest that in an acute phase of vascular injury, changes in permeability occur first and precede formation of vascular remodeling. Whether increased permeability will be followed by

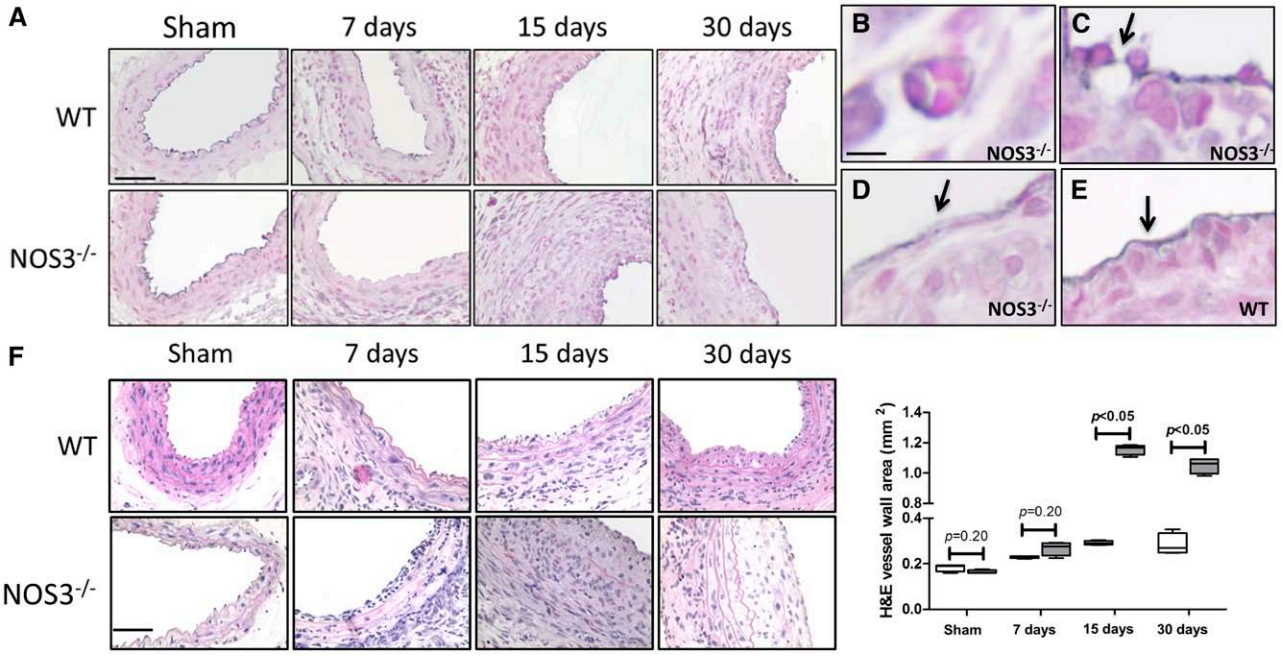

Figure 5. Re-endothelization is impaired in NOS3-knockout (NOS3$^{-/-}$) after endothelial denudation. **A**, PECAM-1 immunohistochemistry (n=3) shows impaired endothelial cell regeneration in NOS3$^{-/-}$ animals when compared with wild-type (WT) mice after endothelial denudation (black, PECAM-1; pink, nuclei). **B**, Histological identification of neovessels (positive for PECAM-1) in NOS3$^{-/-}$ mice at 15 and 30 days after endothelial denudation. Examples of endothelial disruption (**C**; arrow) and denudation (**D**; arrow) in NOS3$^{-/-}$ 30 days after injury using PECAM-1 immunochemistry. **E**, WT mice show endothelial cell regeneration. **F**, Hematoxylin and eosin stain (H&E; n=4) shows larger areas with vascular remodeling and an increased vessel wall area in NOS3$^{-/-}$ mice when compared with WT animals. Scale bars correspond to 0.3 mm. NOS3 indicates endothelial nitric oxide synthase.

remodeling may partly depend on the subsequent re-endothelialization of the vessel wall. However, after the acute phase of endothelial injury (7 days), DE-MRI was in good agreement with vascular remodeling quantified by histology. For this reason, the differences in the long-term vascular response between NOS3$^{-/-}$ and WT mice could be deciphered. NOS3$^{-/-}$ mice showed persistently higher R_1 values and vessel wall enhancement on DE-MRI at 15 and 30 days after injury, which correlated with histological measures of both vascular permeability and remodeling, respectively. Conversely, R_1 and DE-MRI values decreased close to baseline levels in WT animals. It is unclear if gadofosveset interacts nonspecifically with matrix proteins or other components of the vessel wall, but in our previous publication, we have shown that gadofosveset accumulates within the vessel wall without showing preferential localization in specific plaque components using x-ray film gadolinium spectra.[33] In this study, we propose that longitudinal measurements of both vascular permeability and remodeling in a single MRI examination provide a more comprehensive understanding of the focal responses of the vessel wall to injury.

Our histological analysis using PECAM-1 immunohistochemistry showed impaired re-endothelialization and neovessel formation only in NOS3$^{-/-}$ mice 15 and 30 days after injury. Ultrastructural description using TEM showed some evidences of morphological changes of the endothelium in both NOS3$^{-/-}$ and WT animals, including large cytoplasmic vacuoles, altered endothelial cells shape, microvilli, and partial fragmentation of elastin fibers. Similar morphological changes have been previously reported in specimens from both animal models[40] and humans[41] with different cardiovascular risk factors. Nevertheless, a comprehensive morphometric and quantitative analysis of the TEM images would be required to elucidate the mechanism responsible for the differences in permeability observed between the 2 strains. Impaired re-endothelialization and increased neovascularization in NOS3$^{-/-}$ mice resulted in increased vascular permeability as measured by EBD and vascular remodeling measured by H&E. These results are in good agreement with previous histological studies that showed the importance of NOS3-derived nitric oxide in a large number of vascular diseases.[15,42]

In our study, in vivo measurements of R_1 are complimentary to that of EBD. Although the 2 techniques rely on the same biological process, the units of each one are not identical and thus cannot be directly compared. The patterns of the changes, however, between animals and time points are similar between these 2 techniques (see Figures 2 and 4A). The measurements of DE-MRI area and H&E expressed in mm^2 might be more suitable for direct comparison (Figures 3 and 5F). However, in our study, the DE-MRI areas measured on consecutive slices along the aorta and were added for each animal to express the extent of vessel wall remodeling occurring in each time point. Conversely, histology was not performed continuously along the entire length of the vessel but rather in small vascular segments of the aorta. For this reason, the DE-MRI area is always larger compared with the reported histological area.

Different pathways exist to transport molecules across the endothelium. The glycocalyx together with vesicular transport and normal breaks in the tight junctions collectively regulate albumin and other solute flux through intact endothelium into the vessel wall of healthy animals.[43] Albumin transport through these pathways may represent intact endothelium, and could justify the low vessel wall enhancement observed in the DE-MRI and R_1 measurements of sham-operated animals and could also partially contribute to the signal observed in injured vessels. Importantly, our study also showed that in addition to these transport pathways, disruption of the structural integrity of the endothelium together with neovascularization after vascular injury, particularly in NOS3$^{-/-}$ animals, significantly increase vascular permeability and albumin leakage into the vessel wall. These vascular changes could be noninvasively quantified by gadofosveset MRI and are corroborated by histology.

Limitations

Although structural changes of the endothelium may be accompanied by functional alterations of the vasodilatory responses, genetic deletion of the NOS3 gene and lack of protein expression makes the vessel wall inherently irresponsive to acetylcholine stimulation. To this end, we did not assess endothelial function in our study. Another limitation of our study is that in the acute phase of vascular injury DE-MRI overestimated the area of vascular remodeling compared with histology. However, after the acute phase of injury, both vascular permeability and remodeling measured in vivo correlated with the corresponding histological measurements.

Conclusions

Measuring vascular permeability and remodeling by gadofosveset-enhanced MRI may provide surrogate markers for the noninvasive direct evaluation of the healing response of the vessel wall after vascular injury. It could also be used for evaluating the efficacy of treatments aimed at promoting re-endothelialization and attenuating vascular remodeling.

Acknowledgments

The authors would like to thank Mónica Gómez Parrizas for providing experimental assistance on different aspects of this work.

Sources of Funding

We acknowledge financial support from (1) the British Heart Foundation (RG/12/1/29262 and PG/10/044/28343), (2) the Centre of Excellence in Medical Engineering funded by the Wellcome Trust and EPSRC (WT 088641/Z/09/Z), (3) the Department of Health via the National Institute for Health Research (NIHR) comprehensive Biomedical Research Centre award to Guy's and St Thomas' National Health Service (NHS) Foundation Trust in partnership with King's College London and King's College Hospital NHS Foundation Trust. The views expressed are those of the authors and not necessarily those of the NHS, the NIHR, or the Department of Health. (4) Ministerio de Economía y Competitividad SAF 2011 to 28375 and (5) European Cooperation in Science and Technology (COST) action TD1007 Bimodal PET-MRI molecular imaging technologies and applications for in vivo monitoring of disease and biological processes.

Disclosures

None.

References

1. Cines DB, Pollak ES, Buck CA, Loscalzo J, Zimmerman GA, McEver RP, Pober JS, Wick TM, Konkle BA, Schwartz BS, Barnathan ES, McCrae

KR, Hug BA, Schmidt AM, Stern DM. Endothelial cells in physiology and in the pathophysiology of vascular disorders. *Blood*. 1998;91:3527–3561.
2. Brodsky SV, Goligorsky MS. Endothelium under stress: local and systemic messages. *Semin Nephrol*. 2012;32:192–198. doi: 10.1016/j.semnephrol.2012.02.005.
3. Wiesmann F, Petersen SE, Leeson PM, Francis JM, Robson MD, Wang Q, Choudhury R, Channon KM, Neubauer S. Global impairment of brachial, carotid, and aortic vascular function in young smokers: direct quantification by high-resolution magnetic resonance imaging. *J Am Coll Cardiol*. 2004;44:2056–2064. doi: 10.1016/j.jacc.2004.08.033.
4. Vita JA, Keaney JF Jr. Endothelial function: a barometer for cardiovascular risk? *Circulation*. 2002;106:640–642.
5. Le Brocq M, Leslie SJ, Milliken P, Megson IL. Endothelial dysfunction: from molecular mechanisms to measurement, clinical implications, and therapeutic opportunities. *Antioxid Redox Signal*. 2008;10:1631–1674. doi: 10.1089/ars.2007.2013.
6. Xu Y, Arai H, Murayama T, Kita T, Yokode M. Hypercholesterolemia contributes to the development of atherosclerosis and vascular remodeling by recruiting bone marrow-derived cells in cuff-induced vascular injury. *Biochem Biophys Res Commun*. 2007;363:782–787. doi: 10.1016/j.bbrc.2007.09.029.
7. Järvisalo MJ, Raitakari M, Toikka JO, Putto-Laurila A, Rontu R, Laine S, Lehtimäki T, Rönnemaa T, Viikari J, Raitakari OT. Endothelial dysfunction and increased arterial intima-media thickness in children with type 1 diabetes. *Circulation*. 2004;109:1750–1755. doi: 10.1161/01.CIR.0000124725.46165.2C.
8. Förstermann U. Nitric oxide and oxidative stress in vascular disease. *Pflugers Arch*. 2010;459:923–939. doi: 10.1007/s00424-010-0808-2.
9. Förstermann U, Münzel T. Endothelial nitric oxide synthase in vascular disease: from marvel to menace. *Circulation*. 2006;113:1708–1714. doi: 10.1161/CIRCULATIONAHA.105.602532.
10. Cui B, Huang L, Fang Y, Guo R, Yin Y, Zhao X. Transplantation of endothelial progenitor cells overexpressing endothelial nitric oxide synthase enhances inhibition of neointimal hyperplasia and restores endothelium-dependent vasodilatation. *Microvasc Res*. 2011;81:143–150. doi: 10.1016/j.mvr.2010.09.009.
11. Moroi M, Zhang L, Yasuda T, Virmani R, Gold HK, Fishman MC, Huang PL. Interaction of genetic deficiency of endothelial nitric oxide, gender, and pregnancy in vascular response to injury in mice. *J Clin Invest*. 1998;101:1225–1232. doi: 10.1172/JCI1293.
12. Lavin B, Gómez M, Pello OM, Castejon B, Piedras MJ, Saura M, Zaragoza C. Nitric oxide prevents aortic neointimal hyperplasia by controlling macrophage polarization. *Arterioscler Thromb Vasc Biol*. 2014;34:1739–1746. doi: 10.1161/ATVBAHA.114.303866.
13. Huang PL, Huang Z, Mashimo H, Bloch KD, Moskowitz MA, Bevan JA, Fishman MC. Hypertension in mice lacking the gene for endothelial nitric oxide synthase. *Nature*. 1995;377:239–242. doi: 10.1038/377239a0.
14. Cooney R, Hynes SO, Sharif F, Howard L, O'Brien T. Effect of gene delivery of NOS isoforms on intimal hyperplasia and endothelial regeneration after balloon injury. *Gene Ther*. 2007;14:396–404. doi: 10.1038/sj.gt.3302882.
15. Sharif F, Hynes SO, Cooney R, Howard L, McMahon J, Daly K, Crowley J, Barry F, O'Brien T. Gene-eluting stents: adenovirus-mediated delivery of eNOS to the blood vessel wall accelerates re-endothelialization and inhibits restenosis. *Mol Ther*. 2008;16:1674–1680. doi: 10.1038/mt.2008.165.
16. Gauthier TW, Davenpeck KL, Lefer AM. Nitric oxide attenuates leukocyte-endothelial interaction via p-selectin in splanchnic ischemia-reperfusion. *Am J Physiol*. 1994;267:G562–568
17. Marks DS, Vita JA, Folts JD, Keaney JF Jr, Welch GN, Loscalzo J. Inhibition of neointimal proliferation in rabbits after vascular injury by a single treatment with a protein adduct of nitric oxide. *J Clin Invest*. 1995;96:2630–2638. doi: 10.1172/JCI118328.
18. Gerrity RG, Schwartz CJ. Structural correlates of arterial endothelial permeability in the Evans blue model. *Prog Biochem Pharmacol*. 1977;13:134–137.
19. Nguyen PK, Meyer C, Engvall J, Yang P, McConnell MV. Noninvasive assessment of coronary vasodilation using cardiovascular magnetic resonance in patients at high risk for coronary artery disease. *J Cardiovasc Magn Reson*. 2008;10:28. doi: 10.1186/1532-429X-10-28.
20. Terashima M, Nguyen PK, Rubin GD, Iribarren C, Courtney BK, Go AS, Fortmann SP, McConnell MV. Impaired coronary vasodilation by magnetic resonance angiography is associated with advanced coronary artery calcification. *JACC Cardiovasc Imaging*. 2008;1:167–173. doi: 10.1016/j.jcmg.2007.12.001.
21. Hays AG, Hirsch GA, Kelle S, Gerstenblith G, Weiss RG, Stuber M. Noninvasive visualization of coronary artery endothelial function in healthy subjects and in patients with coronary artery disease. *J Am Coll Cardiol*. 2010;56:1657–1665. doi: 10.1016/j.jacc.2010.06.036.
22. Amirbekian V, Lipinski MJ, Briley-Saebo KC, Amirbekian S, Aguinaldo JG, Weinreb DB, Vucic E, Frias JC, Hyafil F, Mani V, Fisher EA, Fayad ZA. Detecting and assessing macrophages *in vivo* to evaluate atherosclerosis noninvasively using molecular MRI. *Proc Natl Acad Sci U S A*. 2007;104:961–966. doi: 10.1073/pnas.0606281104.
23. Botnar RM, Perez AS, Witte S, Wiethoff AJ, Laredo J, Hamilton J, Quist W, Parsons EC Jr, Vaidya A, Kolodziej A, Barrett JA, Graham PB, Weisskoff RM, Manning WJ, Johnstone MT. *In vivo* molecular imaging of acute and subacute thrombosis using a fibrin-binding magnetic resonance imaging contrast agent. *Circulation*. 2004;109:2023–2029. doi: 10.1161/01.CIR.0000127034.50006.C0.
24. Makowski MR, Wiethoff AJ, Blume U, Cuello F, Warley A, Jansen CH, Nagel E, Razavi R, Onthank DC, Cesati RR, Marber MS, Schaeffter T, Smith A, Robinson SP, Botnar RM. Assessment of atherosclerotic plaque burden with an elastin-specific magnetic resonance contrast agent. *Nat Med*. 2011;17:383–388. doi: 10.1038/nm.2310.
25. Winter PM, Morawski AM, Caruthers SD, Fuhrhop RW, Zhang H, Williams TA, Allen JS, Lacy EK, Robertson JD, Lanza GM, Wickline SA. Molecular imaging of angiogenesis in early-stage atherosclerosis with alpha(v)beta3-integrin-targeted nanoparticles. *Circulation*. 2003;108:2270–2274. doi: 10.1161/01.CIR.0000093185.16083.95.
26. Lobbes MB, Heeneman S, Passos VL, Welten R, Kwee RM, van der Geest RJ, Wiethoff AJ, Caravan P, Misselwitz B, Daemen MJ, van Engelshoven JM, Leiner T, Kooi ME. Gadofosveset-enhanced magnetic resonance imaging of human carotid atherosclerotic plaques: a proof-of-concept study. *Invest Radiol*. 2010;45:275–281. doi: 10.1097/RLI.0b013e3181d5466b.
27. Lobbes MB, Miserus RJ, Heeneman S, Passos VL, Mutsaers PH, Debernardi N, Misselwitz B, Post M, Daemen MJ, van Engelshoven JM, Leiner T, Kooi ME. Atherosclerosis: contrast-enhanced MR imaging of vessel wall in rabbit model–comparison of gadofosveset and gadopentetate dimeglumine. *Radiology*. 2009;250:682–691. doi: 10.1148/radiol.2503080875.
28. Phinikaridou A, Andia ME, Passacquale G, Ferro A, Botnar RM. Noninvasive MRI monitoring of the effect of interventions on endothelial permeability in murine atherosclerosis using an albumin-binding contrast agent. *J Am Heart Assoc*. 2013;2:e000402. doi: 10.1161/JAHA.113.000402.
29. Thouet T, Schnackenburg B, Kokocinski T, Fleck E, Nagel E, Kelle S. Visualization of chronic myocardial infarction using the intravascular contrast agent MS-325 (gadofosveset) in patients. *Scientific World J*. 2012;2012:236401. doi: 10.1100/2012/236401.
30. Lauffer RB, Parmelee DJ, Ouellet HS, Dolan RP, Sajiki H, Scott DM, Bernard PJ, Buchanan EM, Ong KY, Tyeklár Z, Midelfort KS, McMurry TJ, Walovitch RC. MS-325: a small-molecule vascular imaging agent for magnetic resonance imaging. *Acad Radiol*. 1996;3 Suppl 2:S356–S358.
31. Caravan P, Cloutier NJ, Greenfield MT, McDermid SA, Dunham SU, Bulte JW, Amedio JC Jr, Looby RJ, Supkowski RM, Horrocks WD Jr, McMurry TJ, Lauffer RB. The interaction of MS-325 with human serum albumin and its effect on proton relaxation rates. *J Am Chem Soc*. 2002;124:3152–3162.
32. Pedersen SF, Thrysøe SA, Paaske WP, Thim T, Falk E, Ringgaard S, Kim WY. CMR assessment of endothelial damage and angiogenesis in porcine coronary arteries using gadofosveset. *J Cardiovasc Magn Reson*. 2011;13:10. doi: 10.1186/1532-429X-13-10.
33. Phinikaridou A, Andia ME, Protti A, Indermuehle A, Shah A, Smith A, Warley A, Botnar RM. Noninvasive magnetic resonance imaging evaluation of endothelial permeability in murine atherosclerosis using an albumin-binding contrast agent. *Circulation*. 2012;126:707–719. doi: 10.1161/CIRCULATIONAHA.112.092098.
34. Lindner V, Fingerle J, Reidy MA. Mouse model of arterial injury. *Circ Res*. 1993;73:792–796.
35. Kumar A, Lindner V. Remodeling with neointima formation in the mouse carotid artery after cessation of blood flow. *Arterioscler Thromb Vasc Biol*. 1997;17:2238–2244.
36. Zhou M, Sutliff RL, Paul RJ, Lorenz JN, Hoying JB, Haudenschild CC, Yin M, Coffin JD, Kong L, Kranias EG, Luo W, Boivin GP, Duffy JJ, Pawlowski SA, Doetschman T. Fibroblast growth factor 2 control of vascular tone. *Nat Med*. 1998;4:201–207.
37. Ali ZA, Alp NJ, Lupton H, Arnold N, Bannister T, Hu Y, Mussa S, Wheatcroft M, Greaves DR, Gunn J, Channon KM. Increased in-stent stenosis in ApoE knockout mice: insights from a novel mouse model of balloon angioplasty and stenting. *Arterioscler Thromb Vasc Biol*. 2007;27:833–840. doi: 10.1161/01.ATV.0000257135.39571.5b.

38. van Beusekom HM, Whelan DM, Hofma SH, Krabbendam SC, van Hinsbergh VW, Verdouw PD, van der Giessen WJ. Long-term endothelial dysfunction is more pronounced after stenting than after balloon angioplasty in porcine coronary arteries. *J Am Coll Cardiol*. 1998;32:1109–1117.
39. van Beusekom HM, van der Giessen WJ, van Suylen R, Bos E, Bosman FT, Serruys PW. Histology after stenting of human saphenous vein bypass grafts: observations from surgically excised grafts 3 to 320 days after stent implantation. *J Am Coll Cardiol*. 1993;21:45–54.
40. Gerrity RG, Richardson M, Somer JB, Bell FP, Schwartz CJ. Endothelial cell morphology in areas of *in vivo* Evans blue uptake in the aorta of young pigs. II. Ultrastructure of the intima in areas of differing permeability to proteins. *Am J Pathol*. 1977;89:313–334.
41. Davies MJ, Woolf N, Rowles PM, Pepper J. Morphology of the endothelium over atherosclerotic plaques in human coronary arteries. *Br Heart J*. 1988;60:459–464.
42. Papapetropoulos A, Rudic RD, Sessa WC. Molecular control of nitric oxide synthases in the cardiovascular system. *Cardiovasc Res*. 1999;43:509–520.
43. Tarbell JM. Shear stress and the endothelial transport barrier. *Cardiovasc Res*. 2010;87:320–330. doi: 10.1093/cvr/cvq146.

CLINICAL PERSPECTIVE

Despite the beneficial effects of percutaneous coronary intervention and stent implantation, these procedures may damage the vessel wall, particularly the endothelial layer, leading to increased vascular permeability and remodeling. Re-endothelialization of the vessel wall with functionally and structurally intact endothelial cells is crucial for minimizing vascular permeability and remodeling and maintaining the long-term patency of the treated vessel. Therefore, longitudinal measurements of both vascular permeability and remodeling in a single MRI examination provide a more comprehensive understanding of the focal responses of the vessel wall to injury. We propose that uptake of gadofosveset, a clinically approved albumin-binding contrast agent, into the vessel wall using T_1 mapping and DE-MRI protocols provides measurements of vascular permeability and remodeling. These biological processes could be used as surrogate markers to assess the healing response of the vessel wall in response to vascular injury.